An Electrical Transient Model of IGBT-Diode Switching Cell for Power Semiconductor Loss Estimation in Electromagnetic Transient Simulation

Yanming Xu, *Student Member, IEEE*, Carl Ngai Man Ho, *Senior Member, IEEE*, Avishek Ghosh, and Dharshana Muthumuni

***Abstract*—An electrical transient model (ETM) of insulated-gate bipolar transistor (IGBT)-diode switching cell is developed by coupling a temperature-dependent IGBT model with power loss model. The nonlinear behavior of IGBT and the reverse recovery characteristic of the diode are considered in this model to simulate the transient switching waveforms. Based on the transient waveforms of ETM under various operating conditions, the power loss estimation method (PLEM) for IGBT is developed. In addition to traditional modeling techniques that only uses ideal switch, this paper uses the model to replicate the power loss behaviors of semiconductor devices in circuit simulation by looking up tables. The proposed ETM is simulated in PSCAD/EMTDC with nanosecond time step, whereas the overall system application can be simulated with conventional time step in range of microsecond. By this way, the model can promise reasonable accuracy as well as an acceptable fast solving speed. The proposed ETM and PLEM have been implemented in PSCAD/EMTDC simulator and validated by experimental results using a double pulse test bench and boost converter test platform.**

***Index Terms*—Diode, electrical transient model, insulated-gate bipolar transistor (IGBT), power loss estimation method (PLEM).**

I. Introduction

POWER semiconductors are critical components in a power electronics (PE) system. Generally, it is the component that limits switching frequency, efficiency, power density, and sometimes reliability in PE converter design [1], [2]. Among modern power semiconductor switches, insulated-gate bipolar transistor (IGBT) is widely used in medium-frequency PE converters ranging from medium to high power. Typically, a converter can contain one IGBT, e.g., boost converter [3], [4], to a few IGBTs, e.g., full bridge inverter [5], to tens of IGBTs, e.g., modular multilevel converter [6]. In a PE converter, an IGBT is paired with a diode in order to provide current commutation for hard switching, this is called "Switching Cell" as shown in Fig. 1 [7] and configured with two structures—negative-cell and positive-cell. During switching transition, heat energy, due to switching losses, is generated in both the IGBT and the diode. The operating junction temperature can vary widely over long period of time, leading to fatigue failure and reduction in the reliability of the entire system. Therefore, PE converter design engineers, researchers, and device manufacturers require an accurate model of IGBT to study its dynamic behavior, and thereby estimate power losses to optimize the system design [8]. It will be the main technological booster for high power applications and help increasing efficiency and optimizing the overall system design.

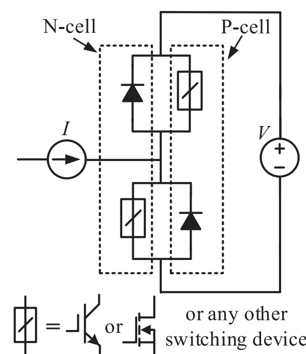

Fig. 1. Switching pattern of the proposed topology.

Several varieties of semiconductor models have been developed. Ideal switch or two-state resistance is employed in most of the electromagnetic transient programs (EMTPs), such as PSCAD/EMTDC and MATLAB/Simulink [9]. It is adequate to evaluate the overall PE system response. However, the switching losses of semiconductor which involve the physics of switching transient have to be considered to assess the efficiency of the PE system [10].

Manuscript received September 21, 2018; revised January 5, 2019 and March 26, 2019; accepted July 4, 2019. Date of publication July 16, 2019; date of current version December 13, 2019. This paper was supported by the Canada Research Chairs Program, Canada, under Grant 950-230361. This paper was presented in part at the IEEE Applied Power Electronics Conference and Exposition, 2018. Recommended for publication by Associate Editor H. Peng. *(Corresponding author: Yanming Xu.)*

Y. Xu, C. N. M. Ho, and A. Ghosh are with the RIGA Lab, the Department of Electrical & Computer Engineering, University of Manitoba, Winnipeg, MB R3T5V6, Canada (e-mail: xuy34527@myumanitoba.ca; carl.ho@umanitoba.ca; ghosha3@myumanitoba.ca).

D. Muthumuni is with the Manitoba HVDC Research Centre, Winnipeg, MB R3P 1A3, Canada (e-mail: dharshana@hvdc.ca).

Color versions of one or more of the figures in this paper are available online at http://ieeexplore.ieee.org.

Digital Object Identifier 10.1109/TPEL.2019.2929113

See http://www.ieee.org/publications_standards/publications/rights/index.html for more information.

To represent the static and dynamic characteristics of IGBT, for most device level studies, IGBT physical models [11], [12] are typically used, such as Hefner model [13], Kuang Sheng model [14], and Kraus model [15]. Those models are based on the device physics to obtain higher accuracy in device simulation, such as Saber and SPICE Model [16], [17]. This imposes a huge computational burden as well as requiring specific dimensions and fabrication description to extract the dedicated physical parameters. Thus, they are generally used in device simulations within one or two switching actions and not suitable for simulating large PE networks. Behavioral models [18], [19], such as Sudhoff model [20] and Hammerstein model [21], ignoring device physics are more convenient with fast simulation speed. However, it cannot represent the detailed switching transient without considering the effect of parasitic parameters and reverse recovery of diode, which is significant for estimating switching losses in various operating conditions. Electrothermal models [22]–[24] considering electrical and thermal couplings involved in the system are able to help solving heat-flow problem and taking temperature effect into account. However, multidimensional thermal model and package properties consideration will increase the complexity of the model which is difficult to implement in the simulator. The choice of IGBT model depends on the required accuracy, complexity, convergence properties, and simulation time.

For accurate estimation of power loss, one approach is curving fitting the loss curve directly or deriving specially defined analytical loss equations based on the switching transient waveforms from measurement, datasheet, or device simulation [25]–[28]. In this way, the accuracy is limited by the specific operating conditions and a mass of device test may be involved. Electromagnetic transient (EMT) simulation-based loss calculation methods [29], [30] use specially developed algebraic equations to piecewise linearize the switching waveforms and externally estimate the device losses with simple switches in system simulation. However, it involves complicated mathematical formulae and parameter extractions without enough temperature consideration. Besides, IGBT TSEPs, such as ON-state voltage (v_{cesat}), threshold voltage (V_t), transconductance (K_p) will change depending on the operating temperature, which also should be considered [31], [32].

This paper proposes a comprehensive PE system simulation method, which uses temperature-dependent electrical transient model (ETM) to simulate static and dynamic behaviors of IGBT-diode switching cell in order to determine semiconductor losses during the PE system simulation. There are two technical contributions in this paper.

1) An IGBT-diode switching cell behavioral model is proposed. Various parameters including tail current, miller plateau voltage, nonlinear parasitic elements of IGBT, and reverse recovery current of diode have been taken into account. All the parameters of the model are extracted from device datasheet considering the temperature sensitivity.
2) A power loss estimation method (PLEM) is developed based on the transient simulation waveforms to calculate the power dissipation of IGBT and diode. And the loss information is connected to the EMTPs circuit simulator, e.g., PSCAD with simple switch model through look up table in PE system simulation. In other words, the switching loss models are integrated into the software (PSCAD) and the system simulation process.

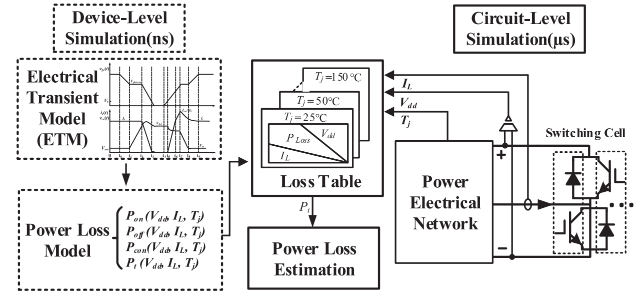

Fig. 2. Block diagram of power loss estimation in a circuit simulation.

With this approach, the speed of PE simulation can be maintained and acceptable accuracy of power loss estimation can be achieved. The model parameter extraction sequence has also been developed to characterize various IGBTs based on the device datasheet. The completed model and method were implemented in PSCAD/EMTDC and verified by experimental results using a double pulse test bench as well as a boost converter test bed.

II. Simulation Strategy of Power Semiconductor Losses

In order to provide fast and accurate semiconductor loss estimation in a PE circuit simulation in an EMTP simulator, e.g., PSCAD, a simulation strategy is proposed. A simplified block diagram of the proposed simulating process including two stages in the simulating platform is shown in Fig. 2.

A. Device Level Simulation

Before simulating an overall PE system, a device level simulation will be done to create four-dimensional (4-D) look-up-tables (LUT) representing transient losses. It generates the loss tables including turn-ON, turn-OFF, reverse recovery, and conduction losses based on the simulation conditions [e.g., junction temperature (T_j), voltage (V_{dd}), and current (I_L)] and power device parameters [e.g., input capacitance (C_{iss}), reverse recovery peak current (I_{rm})]. The semiconductor parameters which are extracted from the datasheet by curve fitting or empirical formulas and the simulation conditions are the inputs to the proposed IGBT-diode switching cell ETM for simulating the detailed switching waveforms. Based on the waveforms, the power losses under various operating conditions which export as a power loss table can be computed by the PLEM. The ETM and the PLEM are applied in the device simulation with nanosecond (ns) time step for the reason of high accuracy. Since only several tens of points will be simulated, it will require only a short computational time.

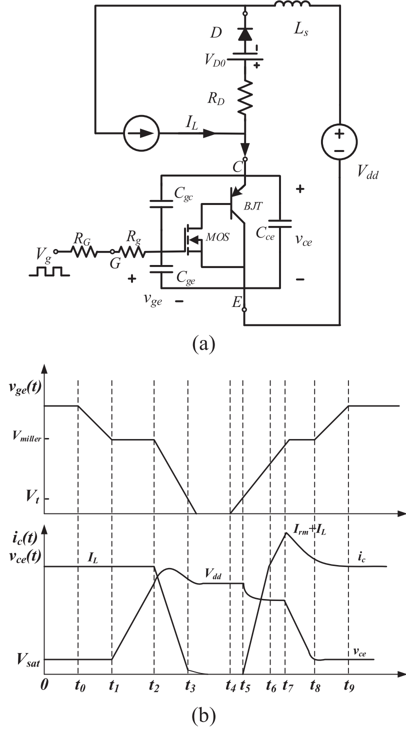

Fig. 3. Switching cell. (a) Equivalent circuit and (b) switching waveforms.

B. Circuit Level Simulation

The obtained LUT in device level simulation works as an interface between the simulations of device and circuit levels. PSCAD simulates the system using an ideal switch model in microsecond (μs) time-step. It inputs instantaneous T_j, V_{dd}, and I_L values to the LUT during each switching action, and computes switching loss and conduction power by interpolation. Furthermore, time-varying instantaneous power loss waveforms can be obtained by taking the integral of the energy loss information, which will provide both static and dynamic system loss information to users. This is a simple search method and mathematics, and will not significantly increase the computational time when comparing to the current PSCAD simulator that uses an ideal model or involving device simulation in circuit simulations.

III. Development of Electrical Transient Model of IGBT-Diode Switching Cell

A diode-clamped inductive load test circuit as shown in Fig. 3(a) is used to investigate the dynamic behaviour of IGBT, and its typical switching waveforms are shown in Fig. 3(b), where V_{dd} is the dc-link voltage and V_g is the gate signal of IGBT. This circuit is implemented to simulate the working operation of IGBT under inductive load condition. The inductive load is large enough to maintain the current constant during one switching cycle which can be considered as current source here. The process and modeling of ETM are illustrated in detail as follows.

The behavioral ETM can give a fast and relatively accurate result for achieving the purpose of estimating switching losses of an IGBT switching cell. ETM can be developed by analyzing the typical switching waveforms of the switching cell. The waveforms are one switching cycle including two switching actions, turn-OFF $(t_0 - t_4)$ and turn-ON $(t_4 - t_9)$ [33]–[35].

A. Switching Process Analysis and Modeling

At t_4 in Fig. 3(b), a turn-ON gate signal $(V_{\rm g})$ is given through the gate resistance including internal and external gate resistance $(R_{\rm gate} = R_g + R_G)$ to charge the input capacitance $(C_{iss} = C_{gc} + C_{ge})$. The rise of gate-emitter voltage (v_{ge}) can be well approximated by a first-order *RC* circuit. The time constant of v_{ge} rising is $\tau = R_{\rm gate} \cdot C_{iss}$. If parasitic inductance is ignored, the gate charging current i_g can be expressed as follows:

$$i_g = C_{iss} \cdot \frac{dv_{ge}}{dt} = \frac{V_g - v_{ge}}{R_{\rm gate}}. \tag{1}$$

Once v_{ge} crosses V_t, the conducting MOS channel is built and the current mainly controlled by the collector–emitter voltage v_{ce} and v_{ge} starts flowing through the IGBT. The static characteristic of IGBT in the regions of cut-off, active, and saturated can be described by the equations in (2), i_{MB} is the total current flowing through the MOS channel and bipolar junction transistor (BJT). Instead of the transconductance K_p in MOS and current gain β in BJT, this paper uses the equivalent trans-conductance, *K*, where $K = (1+\beta) \cdot K_p$. Both *K* and V_t can be extracted directly from the output and transfer characteristics in datasheet

$$i_{MB} = \begin{cases} 0, \; v_{ge} \le V_t \\ K \cdot (v_{ge} - V_t - 0.5 v_{ce}) \cdot v_{ce}, \; v_{ce} \le v_{ge} - V_t \\ 0.5K \cdot (v_{ge} - V_t)^2, v_{ce} > v_{ge} - V_t. \end{cases} \tag{2}$$

Due to stray inductance L_s and the increasing i_c, v_{ce} will have a drop as expressed by

$$v_{ce} = V_{dd} - L_s \frac{di_c}{dt}. \tag{3}$$

As for the nonlinear parasitic capacitance in IGBT, the value of C_{gc} (miller capacitance) will change a lot based on v_{ce}, according to the capacitance curve and gate charging curve in datasheet. Thus, v_{ge} is clamped to a constant value in a period called miller plateau [$t_1 - t_2$ and $t_7 - t_8$ in Fig. 3(b)]. During this period, IGBT keeps conducting and operates in the saturated region. Thus, the voltage source of miller plateau can be described as the following equation, where I_L is the conducting load current:

$$v_{\rm miller} = \sqrt{\frac{2I_L}{K}} + V_t. \tag{4}$$

Because of the minority carrier storage on both sides of the PN junction, the diode cannot switch OFF immediately. Hence, when i_{MB} reaches the value of load current, the diode will undergo reverse recovery as shown in Fig. 4. I_D is the forward conducting current, di_D/dt is the slope of forward current, t_{rr} is the reverse recovery time, and Q_{rr} is the reverse recovery charge. The time at which current enters reverse recovery phase is t_{re}. At t_{rm}, current reaches the reverse peak I_{rm}. For simulating this characteristic, the ETM of diode, which consists of an

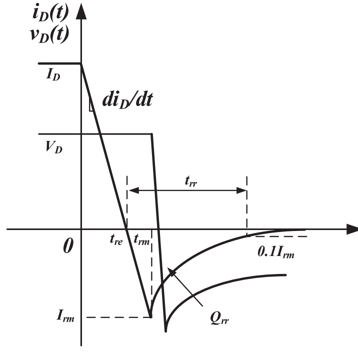

Fig. 4. Reverse recovery characteristic of diode.

ideal diode, forward conducting resistance, R_D, and a reverse recovery current source i_{Dre} has been developed [36].

In a switching cell, current will go through IGBT and diode alternatively. Hence, every time the diode turns OFF and starts reverse recovery, an additional over current will add to the paired IGBT. This interaction is expressed in (5) and the parameters are calculated by (6) according to the datasheet. i_{Dre} is the reverse recovery current of the free-wheeling diode. The decay time constant of the reverse recovery τ_{re} and R_D can be extracted from diode curve using curve fitting

$$i_{Dre} = \begin{cases} \frac{di_D}{dt}\left(t - t_{re}\right), t_{re} < t < t_{rm} \\ I_{rm} e^{-\frac{t - t_{rm}}{\tau_{re}}}, t > t_{rm} \end{cases} \tag{5}$$

$$\begin{cases} \tau_{re} = \frac{1}{ln10}\left(t_{rr} - \frac{I_{rm}}{\frac{di_D}{dt}}\right) \\ I_{rm} = \sqrt{Q_{rr} \cdot di_D/dt} \\ t_{rr} = 2\sqrt{Q_{rr}/di_D/dt}. \end{cases} \tag{6}$$

As soon as the reverse recovery current of diode reaches peak value, v_{ce} drops to the forward conducting voltage v_{cesat}. Meanwhile, v_{ge} increases slowly until it climbs to V_g.

The turn-OFF process is almost the inverse sequence of the turn-ON process, except the tail current period. During the IGBT turn-OFF transient, the excess base carrier recombination makes the shutdown current tailing time longer. Besides the conventional equations, an additional equation has been derived to completely represent this nonlinear characteristic in ETM. In the calculation, the tail current can be described by the exponential function (7). τ is the carrier transit time. t is the simulation time and t_0 is the initial time of the tail current. I_{tail0} is the collector current at the start of the tailed stage

$$i_{MB} = I_{\text{tail }0} \cdot e^{-\frac{t - t_0}{\tau}}, (v_{ge} < V_t, \quad \text{Turn off}). \tag{7}$$

B. Temperature Sensitive Parameters Consideration

TSEPs are today widely used for temperature measurement. With various temperature, electrical parameters of IGBT, such as v_{cesat}, V_t, K, and carrier lifetime (τ), will change and affect the dynamic behavior. Thus, it also should be under consideration for high accuracy simulation. Therefore, this paper uses a series of following equations to describe the TSEPs in IGBT and diode. It should be noted that all the equations are based on the experimental measurement and curve fitting as a function of temperature and various parameters [31]

TABLE I
TSEPS OF IGBT AND DIODE

Parameter	Value	Parameter	Value
V_{t0}	5.812	I_{rm0}	17.77
K_t	0.009988	t_{rm}	0.01234
K_0	2.834	K_{rm}	0.04136
V_{cesat0}	0.9715	K_{trm}	0.000035
r_0	0.02153	Q_{rr0}	3.602
ΔV_{cesat}	-0.001	t_{Qrr}	0.0003
Δr_0	0.0001059	K_{rr}	0.03
T_a	25 ºC	$K_{Q_{rr}}$	0.00000722

TABLE II
PARAMETERS OF DEVICE AND TEST BED

Parameter	Value	Parameter	Value
R_g	6 Ω	C_{iss}	2500 pF
V_t	5.8 V	C_{rss}	110 pF
K	2.834 A/V²	R_G	15 Ω
V_{dd}	0-1 kV	L_l	5 mH
I_L	0-80 A	L_s	180 nH

$$\begin{cases} V_t = V_{t0} - K_t \cdot (T_j - T_a) \\ K = K_0 \cdot \left(\frac{T_a}{T_j}\right)^{0.8} \\ \tau = 5 \times 10^{-7} \cdot \left(\frac{T_a}{T_j}\right)^{1.5} \end{cases} \tag{8}$$

$$\begin{cases} V_{cesat} = (V_{cesat0} + r_0 i_c) + (\Delta V_{cesat} + \Delta r_0 i_c)(T_j - T_a) \\ I_{rm} = I_{rm0} + t_{rm}\frac{di_D}{dt} + \left(K_{rm} + K_{t_{rm}}\frac{di_D}{dt}\right)(T_j - T_a) \\ Q_{rr} = Q_{rr0} + t_{Qrr}\frac{di_D}{dt} + \left(K_{rr} + K_{Q_{rr}}\frac{di_D}{dt}\right)(T_j - T_a). \end{cases} \tag{9}$$

T_a is the initial ambient temperature. T_j is the operating junction temperature. All the curve fitting parameters can be obtained from datasheet. According to (8) and (9), TSEPs can be calculated under various junction temperature and operating conditions and input to switching transient simulation in PSCAD/EMTDC. The TSEPs of the model are extracted from the junction temperature related curves in datasheet of Infineon IKW40T120 IGBT using MATLAB for curve fitting as shown in Table I.

C. Proposed Model Circuit of IGBT and Diode

IGBT is pseudo Darlington structure, which consists of an N-channel MOSFET and a PNP BJT, whose base current is controlled by the MOSFET gate voltage. Based on that, the corresponding schematic of the proposed ETM of an IGBT and a diode are shown in Fig. 5. L_s is the circuit parasitic inductance. The equivalent miller-plateau voltage source v_{miller} works during miller plateau time mentioned above. Also the conducting voltage source v_{cesat} operates during IGBT conducting period. The ETM is formulated in PSCAD/EMTDC including main circuit,

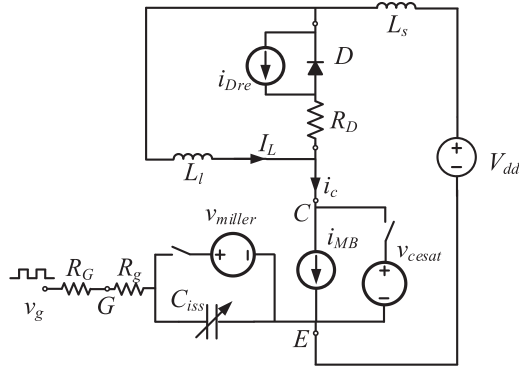

Fig. 5. Proposed transient model circuit of IGBT-diode switching cell.

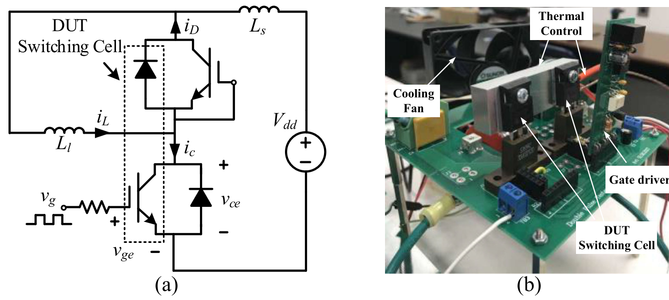

Fig. 6. Loss evaluation setup. (a) Circuit schematic. (b) Test bench.

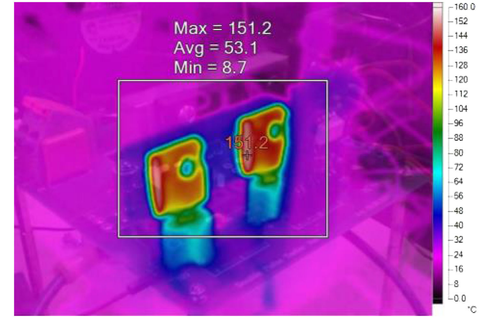

Fig. 7. Thermal image of DUT in DPT.

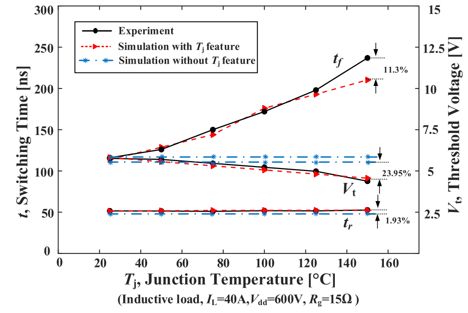

Fig. 8. Switching time and V_t versus T_j.

custom programed models, and other signal control components. The main circuit is implemented by basic electronic components with controlled voltage and current source. The value of TSEPs are updated and calculated by the custom programed model based on the temperature feature and the input operating conditions. Furthermore, the nonlinear features of IGBT and reverse recovery characteristic of body diode are also programed using FORTRAN to control the voltage and current source, respectively. Thus, the transient waveforms of switching cell can be simulated and the switching time as well as other transient parameters can be further extended to power loss calculation model.

IV. Power Loss Estimation Method of IGBT-Diode Switching Cell

Once the switching transient waveforms are obtained by the ETM mentioned in the previous section, the PLEM is developed to analyze and calculate the power loss of IGBT. For simplicity, in Fig. 3(b) the voltage and current are assumed piecewise linear changing except in region t_3 to t_4 and t_7 to t_9. The tailing time, t_{tail}, is defined as the time period when i_c decreases from 10% I_L to 1% I_L. In addition, the diode reverse recovery is very short after t_7 and the loss is neglected. All the following switching period in the expressions can be obtained in the ETM simulation [37].

The main part of the power loss during turn-OFF period occurs from t_1 to t_3 and the tailing current period in Fig. 3(b). The total turn-OFF loss includes the voltage slope loss $E_{\text{off }V}$, the current slope loss $E_{\text{off }I}$, and the tail current loss, $E_{\text{off }T}$.

In the interval $[t_1,\ t_2]$, the current i_c has the same value as I_L and the voltage v_{ce} increases from 0 to V_{dd}. Therefore, the power loss during this period $t_{\text{off }V}$ is given by

$$E_{\text{off }V} = 0.5 I_L V_{dd} t_{\text{off }V}. \tag{10}$$

If v_{ce} is assumed constant during the interval $[t_2,\ t_3]$, the resulting power loss is

$$E_{\text{off}I} = \frac{I_L V_{dd}}{2} \cdot t_{\text{off }I} + 0.5 L_s I_L^2. \tag{11}$$

Assuming the current starts tailing when 10% of I_L and the time constant τ equals to $t_{\text{tail}}/ln10$, the power loss caused by the tail current during the period t_{tail} can be estimated as follows:

$$E_{\text{off}T} = V_{dd} \int_0^{t_{\text{tail}}} e^{-\frac{t}{\tau}} dt = \frac{0.456 I_L V_{dd}}{t_{\text{tail}}}. \tag{12}$$

A similar analysis is carried out to calculate the turn-ON power loss from t_5 to t_8. The total turn-ON power loss includes the current slope, $E_{\text{on }I}$, the voltage slope, $E_{\text{on }V}$ and the reverse recovery loss $E_{\text{on }irr}$.

The power loss for the interval $[t_5,\ t_6]$ characterized by increasing i_c can be expressed as follows:

$$E_{\text{on}I} = 0.5 I_L V_{dd} t_{\text{on }I} - 0.5 L_s I_L^2. \tag{13}$$

Assuming that the current $i_c = I_L$ during the voltage slope interval $[t_7,\ t_8]$, the power loss becomes

$$E_{\text{on}V} = 0.5 I_L V_{dd} t_{\text{on }V}. \tag{14}$$

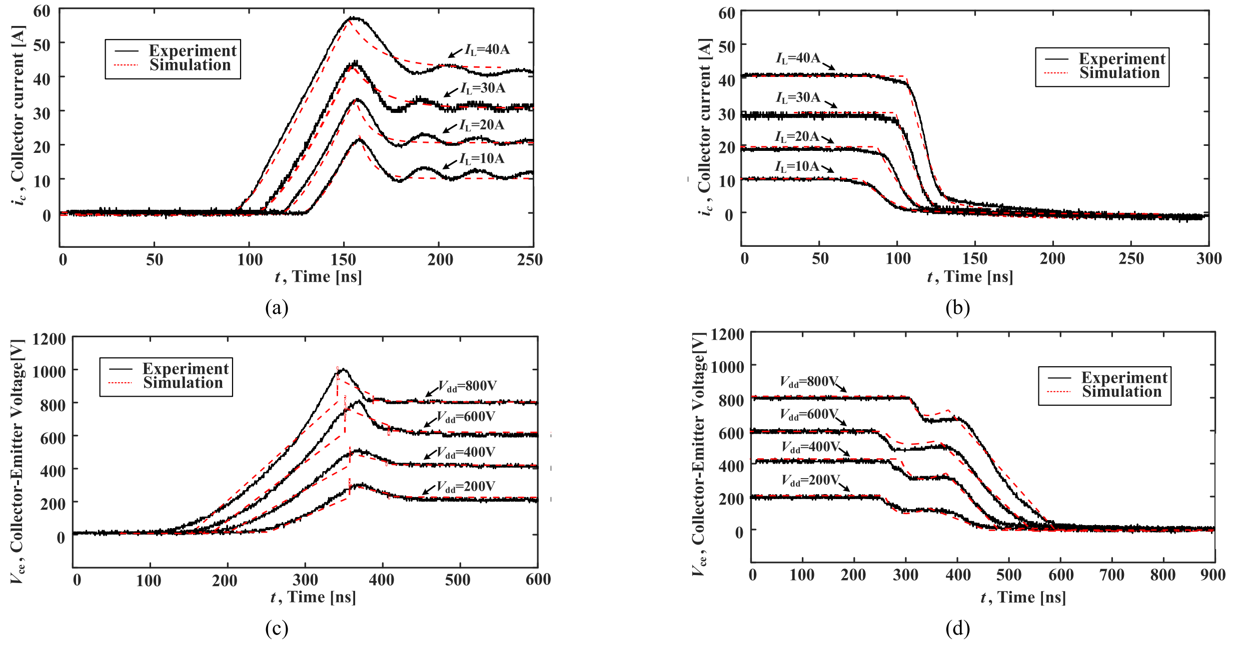

Fig. 9. Switching waveforms. (a) Turn-ON current, (b) turn-OFF current, (c) turn-ON voltage, and (d) turn-OFF voltage.

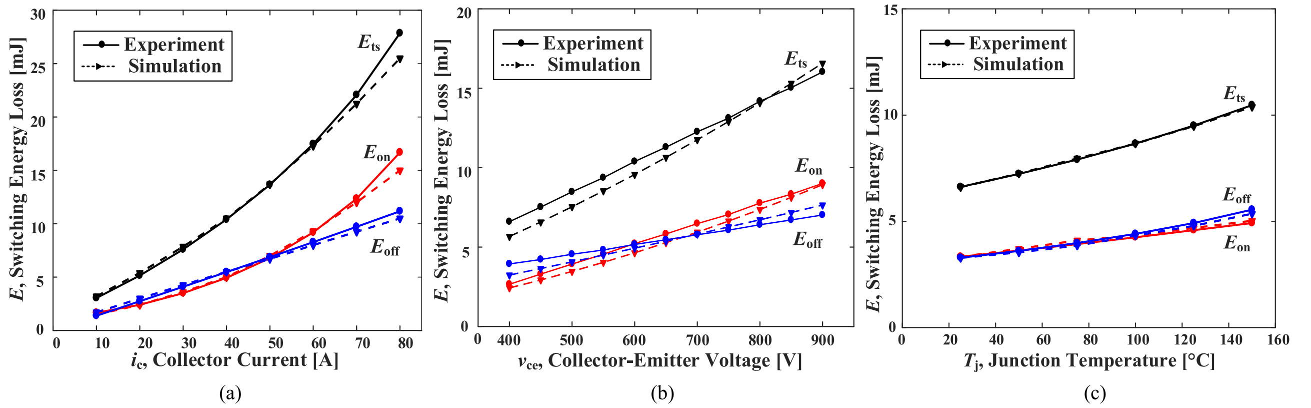

Fig. 10. Switching loss. (a) Versus i_c, (b) versus v_{ce}, and (c) versus T_j.

As for the diode reverse recovery power loss during the period t_{rr}, we assume it is very short with respect to the voltage slope interval. Under this assumption, the power loss caused by the reverse recovery charge Q_{rr} is given by

$$E_{\text{on}irr} = \left(V_{dd} - \frac{L_s I_L}{t_{\text{on}\ I}}\right)(I_L \cdot (t_{rm} - t_{re}) + Q_{rr}). \tag{15}$$

From the output characteristics of IGBT and diode in datasheet, the ON-state voltage can be represented in terms of ON-state zero current collector–emitter voltage V_{ce0} and resistance r_c

$$v_{cesat} = V_{ce0} + r_c i_c. \tag{16}$$

If the average current is I_{cav} and the rms value is I_{crms}, then the average conduction loss of IGBT is as following, where f_{sw} is the switching frequency of IGBT

$$P_{c\text{IGBT}} = f_{\text{sw}} \int_0^{1/f_{\text{sw}}} v_{ce} i_c dt = V_{ce0}\, I_{cav} + r_c I_{c\,\text{rms}}^2. \tag{17}$$

The total switching power loss E_{ts} can be estimated as the sum of the loss equations above, and the total IGBT loss power is expressed in the following equation:

$$E_{ts} = E_{\text{off}V} + E_{\text{off}I} + E_{\text{off}T} + E_{\text{on}I} + E_{\text{on}V} + E_{irr}. \tag{18}$$

From the observation of the set of equations above, V_{dd} and I_L are the key parameters affecting the power loss. In addition, the effects of diode reverse recovery current, parasitic stray inductance, and tail current must also be considered at high switching frequency.

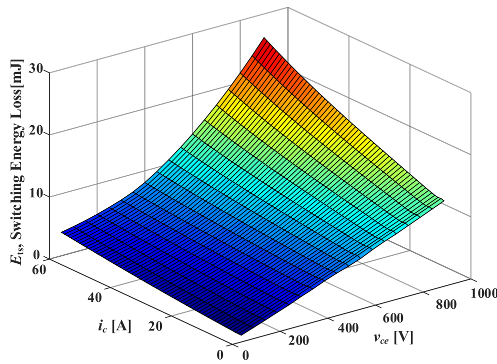

Fig. 11. 3-D plot of switching loss ($T_j = 150\ ^\circ$C).

V. Implementation in Simulator and Experiment Verifications

The ETM and PLEM have been proposed in this paper. The key objective of the model and the method is to estimate the power dissipation of semiconductors in a PE system simulation based on the ETM waveforms. The model and the method are implemented in PSCAD/EMTDC and validated by comparing with the experimental results of double pulse tester and a boost converter. Generally, to use the proposed model, the parameters of the selected Si IGBT device need to be extracted from its datasheet by curve fitting or mathematic methods. Then, the device simulation can be multiple run with ns time step according to the setting range of the operating conditions. The power loss data based on the simulated waveforms can be further exported and reformatted as look up table for power loss prediction in system simulation.

A. Device Level Model Validation

Based on the circuit in Fig. 6(a), a double pulse test (DPT) bench is designed and implemented for characterization of the IGBT and the diode. The test setup consists of power supply, digital signal processing (DSP) control system, thermal control system, cooling fan and the device under test (DUT) as shown in Fig. 6(b). A thermocouple is placed between heatsink and the IGBT device to measure the case temperature. Through the thermocouple amplifier AD595, the value of temperature is further read by the analog pin of DSP. The temperature in DPT is controlled to the test condition by the heater attached to the heatsink and cooling fan as well as the DSP controller. And the thermal imager Tis40 is used in DPT for monitoring the junction temperature of the device.

The Infineon IKW40T120 IGBT device (TO-247 package) is chosen as the DUT. The key parameters of the model and the test bench are listed in Table II. Once the dc capacitor bank is charged to the desired value, a gate signal is given by the DSP to test the behavior of the switching cell. The oscilloscope captures transient switching waveforms. Afterward, a comparison is obtained between the experimental results and the simulation results of the proposed model in PSCAD/EMTDC.

In order to study the temperature-dependent feature, the operating junction temperature of DUT is controlled by the heater and cooling fan and monitored by thermal imager to the desired test condition as shown in Fig. 7. With the junction temperature increasing, the TSEPs will change and thereby can affect the dynamic behavior of the switching cell as discussed above. As a result, the switching time and threshold voltage vary correspondingly as shown in Fig. 8. Since the traditional model only use the basic parameters usually in $T_j = 25\ ^\circ$C or $150\ ^\circ$C, it cannot represent the dynamic changes in various junction temperature and will cause deviations. The simulation results of the proposed model with temperature feature shows a good agreement with the experiment results.

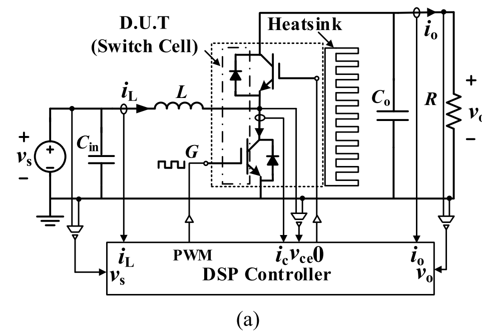

(a)

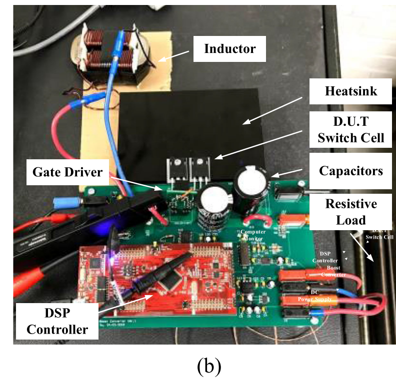

(b)

Fig. 12. Boost converter setup. (a) Block diagram and (b) test bed.

TABLE III
Parameters of Boost Converter

Parameter	Value	Parameter	Value
v_s	150 V	v_o	300 V
L	7.17 mH	C_o	940 μF
R	77 Ω	f_{sw}	10 kHz
Duty cycle	0.5	R_G	15 Ω

Fig. 9 shows the turn-ON and turn-OFF of IGBT collector current and collector–emitter voltage transient waveforms under the test condition ($T_j = 150\ ^\circ$C). The switching details such as current and voltage spikes, tail current, interaction of diode reverse recovery, and the effect of parasitic inductance and capacitance are clearly seen from the transient waveforms. Because of the parasitic parameters of the test bench, there are small oscillations of current after IGBT completely turning ON which is not considered in the model. The PSCAD simulation results show good agreement with the experimental results.

The computed power losses in simulation by PLEM are also compared with the measured results which are obtained by

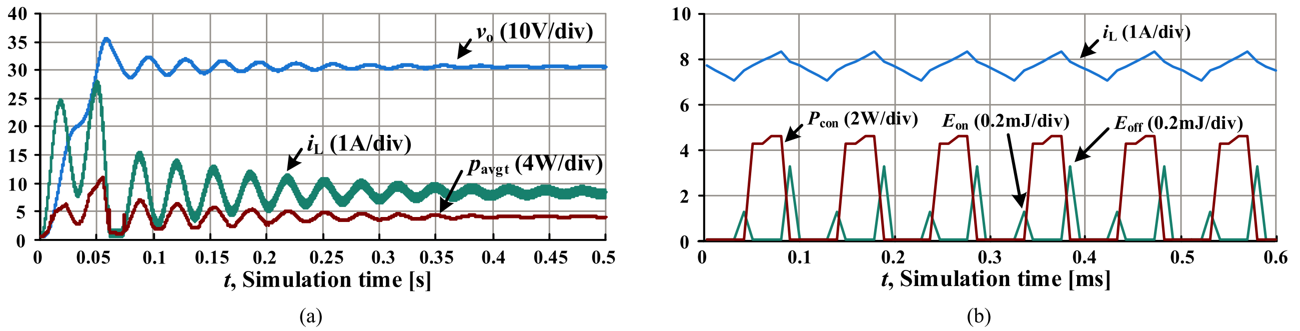

Fig. 13. System simulation. (a) Overall performance and (b) detail power loss.

integrating the product of measured voltage and current during switching process in Fig. 10. A series of load voltage and current can be set to obtain the power loss table by the multiply-run function in PSCAD. As can be seen in Fig. 10, the switching loss changes with the voltage, current, and temperature increasing as well as the proportion of turn-ON and -OFF losses. The simulation results have reasonable accuracy with variation of voltage and current especially in the rated operating condition. Fig. 11 shows an example of a 3-D plot of losses. Although only one layer is graphically demonstrated in Fig. 11, multiple layers with various temperatures are resulted in the simulator. A 4-D table is stored in the simulator and ready for circuit simulations.

B. System Level Model Validation

The proposed model can be applied to various PE applications such as buck or boost converter for semiconductor loss estimation. In order to evaluate the switching cell model and switching losses of a converter simulating in PSCAD, a boost converter, shown in Fig. 12(a), is implemented in PSCAD using the proposed model and methods. The corresponding boost converter test bed with cooling system shown in Fig. 12(b) has been designed and implemented for validation of the simulations. The main parameters of the test bed are listed in Table III. The designed boost converter setup includes the main circuit board, dc power supply, oscilloscope, resistive load, and other measure equipment. The same semiconductor, Infineon IKW40T120 IGBT, is used for testing. Wakefield-Vette 394-2AB heat sink is chosen as the cooling system.

The experiment is conducted at various voltages with a fixed 10 kHz switching frequency controlled by DSP. The same circuit and condition is simulated in PSCAD using the proposed model with standard μs time-step. The overall system performance waveform as well as the details of power loss estimation in simulation is shown in Fig. 13. It can be seen that the detail loss power including turn-ON and OFF power losses and conducting loss power are well estimated during each switching cycle. Fig. 13(a) shows the start-up transient waveforms in the PSCAD simulation. As the output voltage and current increase to steady-state, the inductor current was ringing during the transient and the instantaneous average power can still be estimated and change accordingly. p_{avgt} is the average power loss of power semiconductor in one switching cycle. Fig. 13(b) shows the simulated losses in PSCAD in switching cycle scale for the

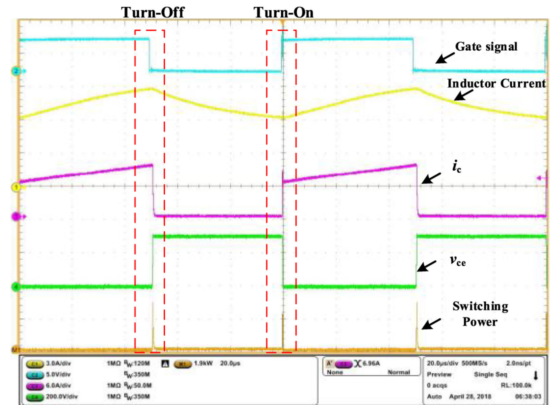

Fig. 14. Measured overall system waveforms of boost converter test bed.

IGBT. During each switching cycle, the turn-ON and turn-OFF losses as well as the conduction power are updated according to the corresponding operating conditions, which validate the dynamic performance of the proposed model.

The measured overall system waveforms in the boost converter test bed are shown in Fig. 14. The detailed turn-ON and turn-OFF waveforms of the IGBT are captured by oscilloscope and shown in Fig. 15(a) and (c), respectively. And the instantaneous switching power can be obtained by the product of v_{ce} and i_c using MATH function in oscilloscope which is then exported and integrated for power loss computing. In order to determine the accuracy of the proposed loss models, the transient waveforms of switching voltage, current, power, and loss under the same test conditions in PSCAD are shown in Fig. 15(b) and (d).

By comparing the experiment and simulation results, it can be seen that the overlap of voltage and current during the switching process correspond to the turn-ON and turn-OFF power losses which are critical, especially when switching frequency increases. The simulation results have good agreement with the experiment results in terms of the dynamic switching turn ON and OFF time as well as the switching loss estimated by the proposed model in simulation.

The junction temperature of IGBT is also monitored by the thermal imager as shown in Fig. 16. Due to the TSEPs' effect as mentioned above, the switching loss also will change a lot with the temperature increasing in Fig. 17. Comparing with power

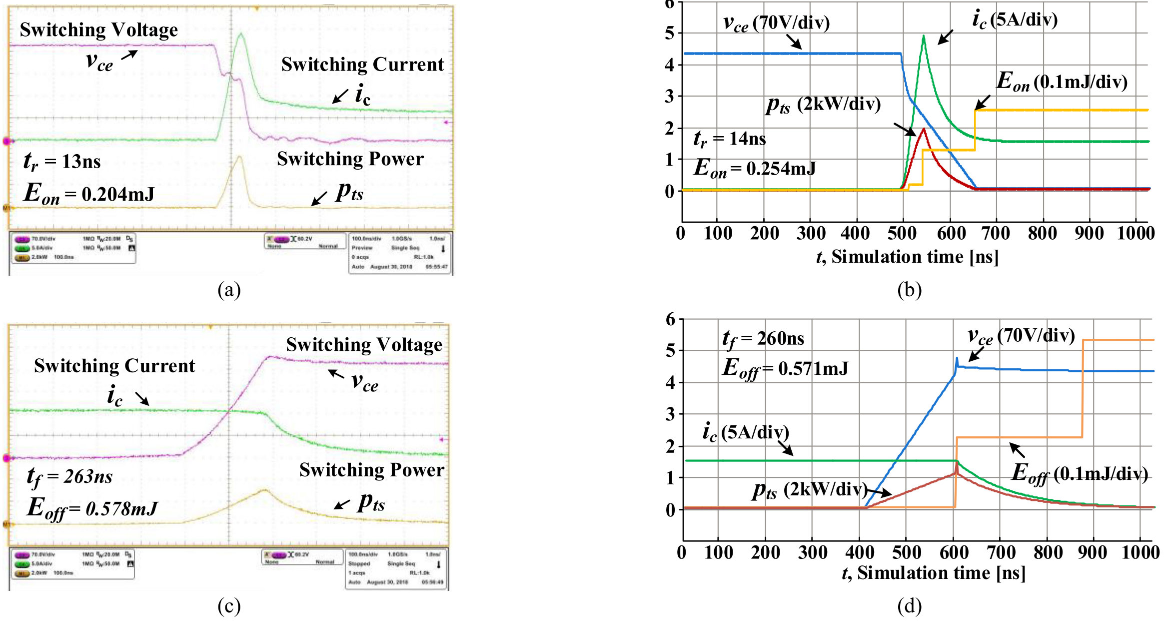

Fig. 15. Turn-ON waveforms. (a) Experiment, (b) simulation, turn-OFF waveforms (c) experiment, and (d) simulation.

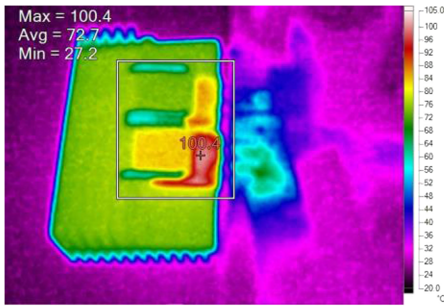

Fig. 16. Thermal image of boost converter.

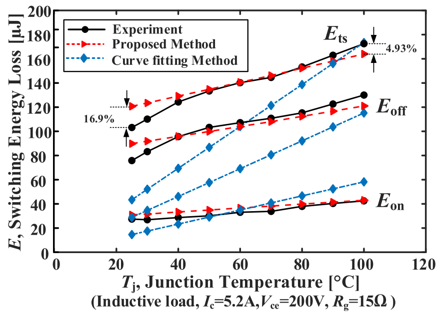

Fig. 17. Switching loss versus T_j.

loss curve fitting method on datasheet which is only linear scaled the effects of temperature and other conditions, the simulation results of the proposed model with temperature feature have better agreement with the experiment results in a wide range of the operating conditions. Although the power loss is analytically estimated by the additional loss table, it is noted that this loss does not affect the electrical circuit simulation.

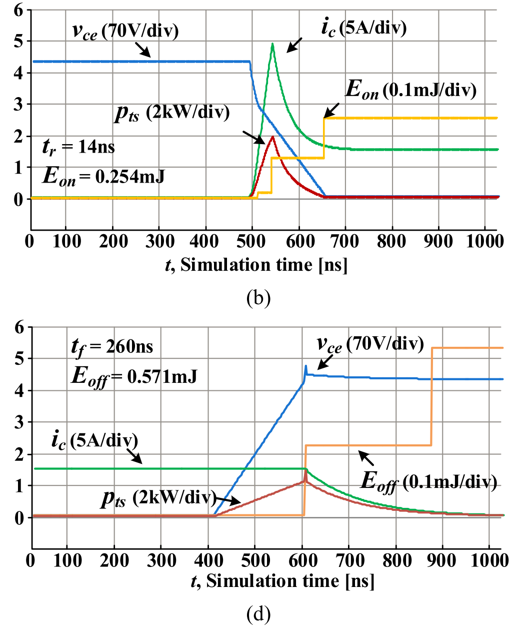

Fig. 18. System simulation time using various models and time step.

C. Discussion of the Model Limitation and Efficiency

The proposed model can be applied to EMT simulator with custom program modeling functions (e.g., PSCAD/EMTDC, MATLAB/Simulink). Junction temperature of the switching cell is considered as a known constant value during the switching cycle and has to be provided by the user.

As for the efficiency of the model, it is a tradeoff between accuracy and speed. The device simulation is recommended to run under ns simulation time step for reasonable accuracy. Therefore, to obtain the power loss look-up table, it needs to choose suitable simulation time step and the operating condition range based on the application which will affect the simulation time and size of the data capacity. Furthermore, comparing with the system simulation time results of various switching models in Fig. 18, it is noted that system simulation using the proposed LUT method with ns time step has a faster simulation speed than using the detail ETM and both of them are only suitable

for a short duration simulation because of the out of memory problem. However, as mentioned above, the proposed model can be run under μs time step with reasonable accuracy by device simulation. In this way, the system simulation can be run for a longer period as well as keeping similar simulation speed comparing with ideal switch.

VI. Conclusion

The paper presented a new simulating approach to obtain semiconductor losses in an EMTP (PSCAD) circuit simulation. The approach can maintain the fast simulating speed as well as reasonable accuracy. The EMTP first creates switching waveforms of the targeting IGBT-diode switching cell in the device-level simulation based on the proposed semiconductor electrical transient model, using the parameters from the device datasheet. Switching losses can be further calculated from the waveforms and stored in a power loss LUT with various conditions. The EMTP starts the circuit-level simulation regularly with simple switch model and obtains power losses in every switching cycle by searching from the LUT. The proposed ETM of IGBT-diode switching cell and PLEM were implemented in PSCAD and successfully resulted semiconductor power losses during circuit simulations. Two hardware test beds have been implemented to evaluate the accuracy of the proposed ETM and PLEM, including a double-pulse tester and a boost converter. The simulation and experimental results show a good agreement. The approach is industry oriented and promising for future high switching frequency converter simulations and system optimizations. It is noted that a suitable selection of simulation time step and operating condition range based on the application in the device-level simulation is still needed which will significantly affect the size of data capacity and simulation time. Moreover, research on close-loop electro-thermal coupling simulation instead of a given constant temperature is required for a better evaluation of efficiency of PE system.

References

[1] Y. Xu, C. Ho, A. Ghosh, and D. Muthumuni, "A behavioral transient model of IGBT module for switching cell power loss estimation in electromagnetic transient simulation," in *Proc. IEEE Appl. Power Electron. Conf. Expo.*, Mar. 2018, pp. 270–275.

[2] N. Iwamuro and T. Laska, "IGBT history, state-of-the-art, and future prospects," *IEEE Trans. Electron Devices*, vol. 64, no. 3, pp. 741–752, Mar. 2017.

[3] C. Ho *et al.*, "Practical design and implementation procedure of an interleaved boost converter using SiC diodes for PV applications," *IEEE Trans. Power Electron.*, vol. 27, no. 6, pp. 2835–2845, Jun. 2012.

[4] S. M. Fazeli, D. Jovcic, and M. Hajian, "Laboratory demonstration of closed-loop 30 kW, 200 V/900 V IGBT-based LCL DC/DC converter," *IEEE Trans. Power Del.*, vol. 33, no. 3, pp. 1247–1256, Jun. 2018.

[5] R. Li, C. Ho, and C. Xu, "Active virtual ground - single phase transformerless grid-connected voltage source inverter topology," *IEEE Trans. Power Electron.*, vol. 33, no. 2, pp. 1335–1346, Feb. 2018.

[6] M. A. Perez, J. Rodriguez, E. J. Fuentes, and F. Kammerer, "Predictive control of AC-AC modular multilevel converters," *IEEE Trans. Ind. Electron.*, vol. 59, no. 7, pp. 2832–2839, Jul. 2012.

[7] F. Z. Peng, L. M. Tolbert, and F. Khan, "Power electronics' circuit topology - the basic switching cells," in *Proc. IEEE Workshop Power Electron. Educ.*, Recife, Brazil, 2005, pp. 52–57.

[8] A. Kopta *et al.*, "Next generation IGBT and package technologies for high voltage applications," *IEEE Trans. Electron Devices*, vol. 64, no. 3, pp. 753–759, Mar. 2017.

[9] A. M. Gole *et al.*, "Guidelines for modeling power electronics in electric power engineering applications," *IEEE Trans. Power Del.*, vol. 12, no. 1, pp. 505–514, Jan. 1997.

[10] H. Selhi and C. Christopoulos, "Generalized TLM switch model for power electronics applications," *Proc. IEE Sci., Meas. Technol.*, vol. 145, no. 3, pp. 101–104, May 1998.

[11] P. Xue, G. Fu, and D. Zhang, "Modeling inductive switching characteristics of high-speed buffer layer IGBT," *IEEE Trans. Power Electron.*, vol. 32, no. 4, pp. 3075–3087, Apr. 2017.

[12] S. Ji, S. Member, Z. Zhao, S. Member, and T. Lu, "HVIGBT physical model analysis during transient," *IEEE Trans. Power Electron.*, vol. 28, no. 5, pp. 2616–2624, May 2013.

[13] A. R. Hefner and D. M. Diebolt, "An experimentally verified IGBT model implemented in the saber circuit simulator," *IEEE Trans. Power Electron.*, vol. 9, no. 5, pp. 532–542, Sep. 1994.

[14] K. Sheng, B. W. Williams, and S. J. Finney, "A review of IGBT models," *IEEE Trans. Power Electron.*, vol. 15, no. 6, pp. 1250–1266, Nov. 2000.

[15] R. Kraus and H. J. Mattausch, "Status and trends of power semiconductor device models for circuit simulation," *IEEE Trans. Power Electron.*, vol. 13, no. 3, pp. 452–465, May 1998.

[16] Y. Duan, F. Xiao, Y. Luo, and F. Iannuzzo, "A lumped-charge approach based physical SPICE-model for high power soft-punch through IGBT," *IEEE Trans. Emerg. Sel. Topics Power Electron.*, vol. 7, no. 1, pp. 62–70, Mar. 2019.

[17] M. Riccio *et al.*, "Accurate SPICE modeling of reverse-conducting IGBTs including self-heating effects," *IEEE Trans. Power Electron.*, vol. 32, no. 4, pp. 3088–3098, Apr. 2017.

[18] C. Liu *et al.*, "FPGA-based real-time simulation of high-power electronic system with nonlinear IGBT characteristics," *IEEE Trans. Emerg. Sel. Topics Power Electron.*, vol. 7, no. 1, pp. 41–51, Mar. 2019.

[19] A. Nejadpak and O. A. Mohammed, "Functional ON/OFF behavioral modeling of power IGBT using system identification methods," in *Proc. 27th Annu. IEEE Appl. Power Electron. Conf. Expo.*, 2012, pp. 1826–1832.

[20] J. L. Tichenor, S. D. Sudhoff, and J. L. Drewniak, "Behavioral IGBT modeling for predicting high frequency effects in motor drives," *IEEE Trans. Power Electron.*, vol. 15, no. 2, pp. 354–360, Mar. 2000.

[21] J. Hsu and K. D. T. Ngo, "Behavioral modeling of the IGBT using the Hammerstein configuration," *IEEE Trans. Power Electron.*, vol. 11, no. 6, pp. 746–754, Nov. 1996.

[22] C. H. van der Broeck *et al.*, "Spatial electro-thermal modeling and simulation of power electronic modules," *IEEE Trans. Ind. Appl.*, vol. 54, no. 1, pp. 404–415, Jan./Feb. 2018.

[23] T. Liang and V. Dinavahi, "Real-time system-on-chip emulation of electrothermal models for power electronic devices via hammerstein configuration," *IEEE Trans. Emerg. Sel. Topics Power Electron.*, vol. 6, no. 1, pp. 203–218, Mar. 2018.

[24] Y. Tang and H. Ma, "Dynamic electrothermal model of paralleled IGBT modules with unbalanced stray parameters," *IEEE Trans. Power Electron.*, vol. 32, no. 2, pp. 1385–1399, Feb. 2017.

[25] S. Dieckerhoff, S. Bernet, and D. Krug, "Power loss-oriented evaluation of high voltage IGBTs and multilevel converters in transformerless traction applications," *IEEE Trans. Power Electron.*, vol. 20, no. 6, pp. 1328–1336, Nov. 2005.

[26] K. Takao and H. Ohashi, "Accurate power circuit loss estimation method for power converters with Si-IGBT and SiC-diode hybrid pair," *IEEE Trans. Electron Devices.*, vol. 60, no. 2, pp. 606–612, Feb. 2013.

[27] A. K. Sadigh, V. Dargahi, and K. A. Corzine, "Analytical determination of conduction and switching power losses in flying-capacitor-based active neutral-point-clamped multilevel converter," *IEEE Trans. Power Electron.*, vol. 31, no. 8, pp. 5473–5494, Aug. 2016.

[28] C. Wong, "EMTP modeling of IGBT dynamic performance for power dissipation estimation," *IEEE Trans. Ind. Appl.*, vol. 33, no. 1, pp. 64–71, Jan./Feb. 1997.

[29] A. D. Rajapakse, A. M. Gole, and P. L. Wilson, "Electromagnetic transients simulation models for accurate representation of switching losses and thermal performance in power electronic systems," *IEEE Trans. Power Del.*, vol. 20, no. 1, pp. 319–327, Jan. 2005.

[30] A. D. Rajapakse, A. M. Gole, and R. P. Jayasinghe, "An improved representation of FACTS controller semiconductor losses in EMTP-type programs using accurate loss-power injection into network solution," *IEEE Trans. Power Del.*, vol. 24, no. 1, pp. 381–389, Jan. 2009.

[31] P. R. Palmer *et al.*, “Circuit simulator models for the diode and IGBT with full temperature dependent features,” *IEEE Trans. Power Electron.*, vol. 18, no. 5, pp. 1220–1229, Sep. 2003.
[32] Y. Avenas, L. Dupont, and Z. Khatir, “Temperature measurement of power semiconductor devices by thermo-sensitive electrical parameters—A review,” *IEEE Trans. Power Electron.*, vol. 27, no. 6, pp. 3081–3092, Jun. 2012.
[33] A. T. Bryant *et al.*, “Two-step parameter extraction procedure with formal optimization for physics-based circuit simulator IGBT and p-i-n diode models,” *IEEE Trans. Power Electron.*, vol. 21, no. 2, pp. 295–309, Mar. 2006.
[34] C. N. M. Ho, F. Canales, A. Coccia, and M. Laitinen, “A circuit-level analytical study on switching behaviors of SiC diodes at basic cell for power converters,” in *Proc. IEEE Ind. Appl. Soc. Annu. Meeting*, Oct. 2008, pp. 1–8.
[35] M. Jin and M. Weiming, “Power converter EMI analysis including IGBT nonlinear switching transient model,” *IEEE Trans. Ind. Electron.*, vol. 53, no. 5, pp. 1577–1583, Oct. 2006.
[36] A. L. I. Dastfan, “A new macro-model for power diodes reverse recovery,” in *Proc. Energy Convers. Congr. Expo.*, 2007, pp. 48–52.
[37] Y. Lobsiger and J. W. Kolar, “Closed-loop IGBT gate drive featuring highly dynamic di/dt and dv/dt control,” *IEEE Trans. Power Electron.* vol. 30, no. 5, pp. 4754–4761, Sep. 2012.

Yanming Xu (S’16) received the B.Eng. and M.Eng. degrees in electronic engineering from the North China Electric Power University, Beijing, China, in 2013 and 2016, respectively. He is currently working toward the Ph.D. degree in power electronics with the University of Manitoba, Winnipeg, MB, Canada.

His current research interests include wide bandgap devices characterization and semiconductor modeling.

Carl Ngai Man Ho (M’07–SM’12) received the B.Eng. and M.Eng. double degrees and the Ph.D. degree in electronic engineering from the City University of Hong Kong, Hong Kong, in 2002 and 2007, respectively.

From 2002 to 2003, he was a Research Assistant with the City University of Hong Kong. From 2003 to 2005, he was an Engineer with e.Energy Technology Ltd., Hong Kong. In 2007, he joined ABB Switzerland. He has been appointed as a Principal Scientist and he has led a research project team at ABB to develop Solar Inverter technologies. In October 2014, he joined the University of Manitoba, Winnipeg, MB, Canada, where he is currently an Associate Professor and Canada Research Chair in Efficient Utilization of Electric Power. He established the Renewable-Energy Interface and Grid Automation (RIGA) Lab, the University of Manitoba, to research on microgrid technologies, renewable energy interfaces, real time digital simulation technologies, and demand-side control methodologies.

Dr. Ho is currently an Associate Editor of the IEEE TRANSACTIONS ON POWER ELECTRONICS (TPEL) and the IEEE JOURNAL OF EMERGING AND SELECTED TOPICS IN POWER ELECTRONICS (JESTPE). He was the recipient of the Best Associate Editor Award of JESTPE in 2018.

Avishek Ghosh received the B.Eng. degree in electronics and electrical engineering with first class honors from the University of Glasgow, Glasgow, U.K., in 2012, and the M.Sc. degree from the Department of Electrical and Computer Engineering from the University of Manitoba, Winnipeg, MB, Canada, in April 2019. He is currently working toward the Ph.D. degree with the Renewable-Energy Interface and Grid Automation (RIGA) Lab, University of Manitoba.

He has worked in the energy sector in India from 2012 to 2016. As a Project Engineer, he gained industrial experience in areas of manufacturing, testing, and commissioning of electrostatic precipitator (ESP) technologies, HV switchgears, and other substation equipments. He is working as a Research Assistant with the RIGA Lab, University of Manitoba. His current research interests include wide-bandgap semiconductor device characterization, and applications and power hardware in the loop simulations.

Dharshana Muthumuni received the Ph.D. degree in electrical engineering from the University of Manitoba, Winnipeg, MB, Canada, in 2001.

He joined the Manitoba HVDC Research Centre (MHRC), Winnipeg, in 2001, and is currently the Managing Director of the Power Systems Technology Centre, Manitoba Hydro International Ltd. He has more than 25 years of experience in engineering studies using a variety of simulation products during his career, including PSCAD and PSS/E./EMTDC. He has led the MHRC technical team to solve challenging engineering problems, including wind farm modeling and integration, SSR, black start restoration, and interconnection issues. He is the MHRC’s Machines and Transformer Modeling and Simulation Specialist and plays an active role in developing new models of power system apparatus for transient simulation studies, working closely with equipment manufacturers to develop detailed simulation models. Some of his work includes the development and validation testing of detailed machine models, transformer and current-transformer saturation routines, development of models for wind power and solar applications, and complex magnetic fault current limiter models.